Proceedings of the 34th European Modeling & Simulation Symposium (EMSS), 016
19th International Multidisciplinary Modeling & Simulation Multiconference

2724-0029 © 2022 The Authors.
doi: 10.46354/i3m.2022.emss.016

Optimization of the Drying Time of Industrial Solvents: Numerical Modelling within COMSOL Multiphysics®

Frédéric VIRY[1,*], Magali STURMA[2], Patrick NAMY[1] and Bruno BARBET[2]

[1]SIMTEC, 5 rue Félix Poulat, 38000 Grenoble, France
[2]MARKEM-IMAJE, 9 rue Gaspard Monge, 26500 Bourg-lès-Valence, France

[*]Corresponding author. Email address: frederic.viry@simtecsolution.fr

Abstract

In the field of industrial inkjet marking, the drying time to evaporate the solvent is a key factor of the process productivity. In order to optimize it, a new approach of the drying process is assessed numerically in this paper. An air blade is used to push away the newly evaporated solvent to reduce the local solvent partial pressure. Therefore, it maximizes the vaporization flux. This idea is implemented within the software COMSOL Multiphysics®. The air flow is computed through the Navier-Stokes equation, and the solvent concentration is modelled by a convection-diffusion equation. The vaporization profile is assessed in several configurations. Eventually, the numerical results show that the air blade reduces dramatically the drying time. By this way and given a drying time in industrial environment, one can consider a broader family of solvent, *i.e.* less volatile solvent compared to so called MethylEthylKetone.

Keywords: Drying time; solvent; COMSOL Multiphysics; numerical modelling

1. Introduction

Inkjet printing technologies aims to coat a media with a liquid layer subsequently becoming solid to prevent any ink bleeding damaging print quality. A broad family of inks are solvent based meaning the dry content remains on the substrate (dye, binder...) while the solvent is evaporated in air especially on non-porous medium. In coding and marking CIJ inkjet technology, media speed is so high (couple of meters per second) that there is no much time to get the solvent evaporated before packing the goods leading to an overwhelming use of MEK solvent (high vapor pressure *i.e.* fast evaporation rate). To overcome the usage of MEK (oil-based solvent) and considering the "green trend", the use of other solvents (*e.g.* water-based solvents) leads unfortunately to have lower evaporation rate (Le, 1999) (Castrejon-Pita, Baster, J., S., & M., 2013). Recent developments include laser heating technologies (Numata, et al., 2013). This article investigates how an air blow purposely designed can modify and ultimately speed-up evaporation time.

2. State of the art

Problem statement has consisted of creating an analytical model to emphasize the physics to be taken into account and to know whether an air flow could enhance the evaporation process.

The analytical model developed is 1D, assuming evaporation direction is only along y axis (perpendicular to liquid surface) as described in Fig. 1. The hydrodynamic layer issued from the air flow at the surface of the liquid surface reads:

$$\delta(x) = \sqrt{\nu/v_j \cdot x}, \quad (1)$$

with v_j the air velocity and ν the kinematic air viscosity.

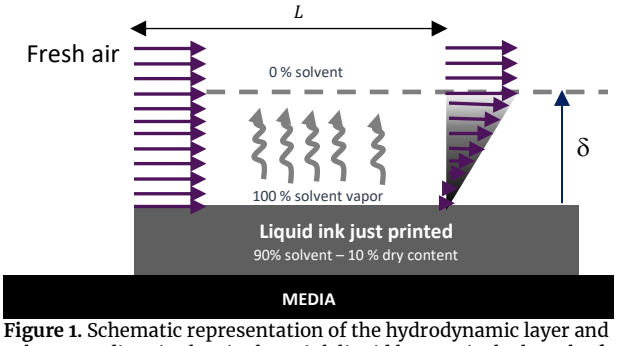

Figure 1. Schematic representation of the hydrodynamic layer and solvent gradient in the air above ink liquid layer. L is the length of hydrodynamic layer expansion (same direction as air flow).

The mass flux of solvent J_m , across the diffusion layer, is driven by the first order Fick's law considering the steady state:

$$J_m = D\frac{\partial c}{\partial y} = D\frac{c_0 - c\big(y=\delta(x)\big)}{\delta(x)}, \tag{2}$$

with D the diffusion coefficient of solvent in air, c the concentration of solvent in air, equaling c_0 at $y = 0$, the liquid surface. Mass of evaporated solvent m_e as function of time t is related to the mass flux:

$$\frac{dm_e}{dt} = J_m \tag{3}$$

Combining Eq. 1-3 and after space integration, drying time T is obtained when the mass of solvent is exhausted from the liquid layer *i.e.*, thickness of ink decreases from e_i down to 0:

$$T = \left(\frac{2}{3}\frac{\rho e_i}{D c_0}\right)\sqrt{\frac{\nu}{v_j}L} \tag{4}$$

Evaporation times decreases as function of air velocity root square. Such a strong importance opens opportunity for industrial implementation and benefit however key parameters such as media velocity or concentration along x axis are overlooked so far, leading to the following numerical model.

3. Materials and Methods

3.1. Physical process description

Fig. 2 exhibits the experimental set-up consisting in an industrial continuous inkjet printer (9450 range Markem-Imaje product) steering some liquid droplets to the media. The dot pattern (individual spot) undergoes the air flow downstream the printhead to dry *i.e.*, extract the solvent from the liquid spot. The air flow is generated by a commercial so called air knife (Exair brand name), the air blade is of 100 µm in thickness providing air velocity in the range of 0 to 100 m/s as function of the inlet pressure. Decision making of dry/wet state consists to wipe the printed spot by a rubber blade at different delay.

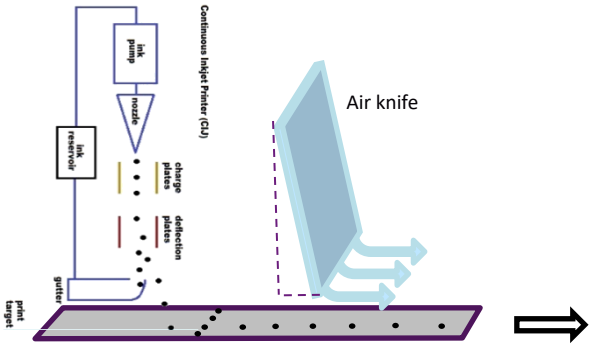

Figure 2. Schematic representation of the experimental device.

To mimic the experimental device in the computational world, Fig. 3 describes the relevant parameters retained such as both air flows issued from the conveyor motion at velocity v_c, and the jet at velocity v_j. Both may be switched on or switched off: $v_c \in \{0, 1\}$ m/s and $v_j \in \{0, 100\}$ m/s.

Figure 3. Schematic representation of the computational domain. Width is 1.64 m and height is 32 cm. The bottom horizontal dashed line represents a conveyor. The air blade (delimited by blue and red lines) is 16 cm long and is oriented 10° relatively to the vertical axis, 1 cm above the conveyor. The end of the air blade (red line) sizes 100 µm.

3.2. Numerical Model

3.2.1. *Air Flow*

The flow is considered here at steady state, with ambient temperature T, 35 °C. The Mach number never exceeds 0.3, so the air flow is modelled by the incompressible Navier-Stokes equations:

$$\begin{aligned} \boldsymbol{\nabla}\cdot\boldsymbol{u} &= 0 \\ \rho\,\boldsymbol{u}\cdot\boldsymbol{\nabla}\boldsymbol{u} &= -\boldsymbol{\nabla}p + \boldsymbol{\nabla}\cdot\left[\mu\left(\boldsymbol{\nabla}\boldsymbol{u} + (\boldsymbol{\nabla}\boldsymbol{u})^{\mathrm{T}}\right)\right] \end{aligned} \tag{5}$$

where $\boldsymbol{u}$ is the air velocity, p the air pressure, ρ the air density, and μ the air dynamic viscosity at ambient temperature respectively.

The velocity v_j is prescribed at the end of the air blade (Fig. 3, red solid line). No-slip boundary conditions are prescribed on the horizontal bottom boundary moving at velocity v_c (Fig. 3, dashed line), and null velocity on the remaining walls of the blade (Fig. 3, blue solid lines). Open boundary conditions are considered on the remaining boundaries to model a non-limited area (Fig. 3, black solid lines).

3.2.2. *Convection-Diffusion of Solvent in Air*

In the air domain (Fig. 3), the solvent concentration c is

transported by air flow, and diffuses:

$$\frac{\partial c}{\partial t} + \boldsymbol{u} \cdot \boldsymbol{\nabla} c = D \Delta c, \tag{6}$$

where D is the homogeneous diffusion coefficient of the solvent in air. Energy transfers occur during phase transition, but these effects are neglected here. The evaporation process of the ink layer is then described by mass transfers from the liquid phase to the gaseous one. At initial state, air is empty of solvent:

$$c(t = 0) = 0. \tag{7}$$

The diluted gas air/solvent is assumed to be an ideal gas. At the interface between the liquid layer and the air, the equilibrium between liquid and gaseous phases is assumed to be reached. Therefore, the solvent partial pressure is equal to the vapor pressure p_{vap} at temperature T, and the solvent concentration c_0 is obtained by the ideal gas law:

$$c_0 = \frac{p_{vap}}{R \cdot T}. \tag{8}$$

The horizontal bottom boundary (Fig. 3, dashed line) is the surface of an impervious solid on which the liquid layer is conveyed at constant velocity v_c. The initial position of the layer on the conveyor is x_0. The layer is not represented geometrically in height, due to its thinness, 10 µm, compared to its width w, 2 cm. On the edge representing the interface between the liquid layer and air, concentration is fixed to c_0:

$$c = c_0 \qquad x \in [x_0 + vt, x_0 + w + vt], \tag{9}$$

while on the remaining parts, the impermeability is modelled by a homogeneous Neumann condition:

$$-D \boldsymbol{\nabla} c \cdot \boldsymbol{n} = 0 \qquad x \notin [x_0 + v \cdot t, x_0 + w + v \cdot t], \tag{10}$$

where $\boldsymbol{n}$ denotes the outward normal vector to the computational domain.

Open boundary conditions are used on remaining boundaries (Fig. 3, solid lines):

$$\begin{array}{ll} -D \boldsymbol{\nabla} c \cdot \boldsymbol{n} = 0 & \boldsymbol{u} \cdot \boldsymbol{n} \geq 0 \\ c = 0 & \boldsymbol{u} \cdot \boldsymbol{n} < 0 \end{array}. \tag{11}$$

3.2.3. Liquid Mass Dynamic and Drying Time

The liquid layer has initially a mass m_0. The dynamic of the liquid layer mass m follows from the mass transfers from liquid phase to gaseous phase:

$$\frac{dm}{dt} = M \int_{liquid\ layer} D \boldsymbol{\nabla} c \cdot \boldsymbol{n} \, \mathrm{d}x, \tag{12}$$

where M is the molar mass of the solvent.

The liquid layer is assumed to be totally evaporated when m becomes equal to zero. The duration to reach this state is called the drying time.

3.2.4. Numerical Implementation

This model is implemented within COMSOL Multiphysics® 5.6 (COMSOL, 2020). All variables are spatially discretized by finite elements, on the mesh illustrated in Fig. 4, which is especially refined near the conveyor in order to accurately solve the flow boundary layer and the diffusion boundary layer, but also at the end of the air blade.

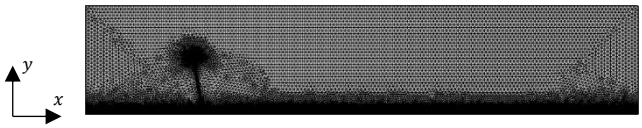

Figure 4. Mesh used for numerical simulation. The mesh is refined near the conveyor, where minimal element size has width of 100 µm and height of 5 µm, and the end of the air blade.

The steady air flow (Eq. 5) is obtained through a transient Navier-Stokes simulation during 5 seconds, starting from air at rest. Boundary conditions on the conveyor and the end of the air blade are modulated by a smooth step function, in order to avoid temporal discontinuities. Air flow variables $\boldsymbol{u}$ and p are spatially discretized using stabilized $P1 + P1$ finite elements (Hughes, Franca, & Balestra, 1986), leading to 1 million of degrees of freedom to solve at each timestep. The time discretization and resolution are performed by a BDF (backward differentiation formula) solver, where a set of nonlinear equations are solved at each timestep by Newton-Raphson method.

The solvent concentration c and the remaining liquid mass m are solved together. c is discretized using $P1$ finite elements, leading to 0.3 million of degrees of freedom to solve at each timestep. High numerical Peclet numbers may be encountered near the conveyor, thus Eq. 2 is stabilized using crosswind diffusion (Do Carmo and Galeão), and streamline diffusion (COMSOL, 2020). A BDF solver is used to for temporal discretization and resolution of Eq. 6 and Eq. 12. Even if Eq. 6-12 were linear, stabilization terms makes the numerical problem to solve at each timestep nonlinear, solved by Newton-Raphson method.

4. Results and Discussion

Evaporation is simulated for 3 scenarios for the MethylEthylKetone: (1) no jet/static conveyor $v_j = 0$ m/s, $v_c = 0$ m/s; (2) no jet/moving conveyor $v_j = 0$ m/s, $v_c = 1$ m/s; and (3) with jet/moving conveyor $v_j = 100$ m/s, $v_c = 1$ m/s. Fig. 5 provides the dynamic of the liquid layer mass m in each case. Table 1 synthetizes the drying time in each case. The relative air/layer edge velocity magnitude, taken at the center of the layer and 100 µm above, is shown in Fig. 6.

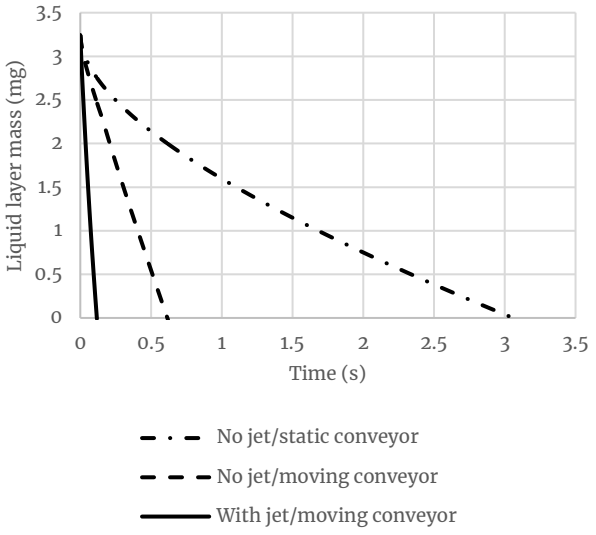

Figure 5. Liquid layer remaining mass along time in each case.

Table 1. Absolute drying time and drying time relatively to case with jet/moving conveyor in each case.

Case	Abs. time (s)	Rel. time (1)
No jet/static conveyor	3.06	26
No jet/moving conveyor	0.62	5.2
With jet/moving conveyor	0.12	1

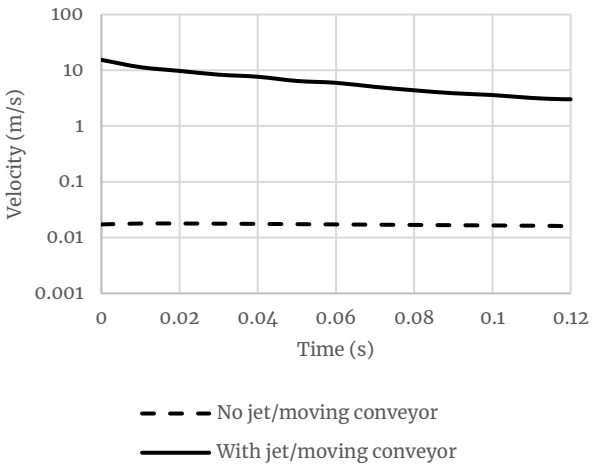

Figure 6. Velocity magnitude of air relatively to the center of the layer edge 100 µm above the conveyor. This quantity is null for the no jet/static conveyor case.

Fig. 5 and Table 1 show that the drying time decreases by switching on the conveyor motion and the jet. This tendency is not surprising and can be understood from the physical model developed here. Eq. 12 states that evaporation can be optimized by maximizing the concentration gradient normally to the conveyor. This is made possible by bringing fresh air ($c \approx 0$) near the liquid layer, since a constant concentration c_0 is prescribed at the liquid/gas interface (Eq. 9). The process of air renewal near the liquid layer is handled by the convection process (Eq. 6). This reasoning allows to correlate the relative air/layer velocity magnitude increase (Fig. 6) to the drying time decrease (Table 1). These results are strengthened by the a priori analysis (Eq. 4).

In an industrial perspective, only the moving conveyor cases are of interest. It is shown in Table 1 that switching on the jet dramatically decreases the drying time by a factor 5. This is an important result, since it makes it possible to consider using less volatile solvents at constant drying time by taking the convection into consideration.

5. Conclusions

A numerical model has been developed to estimate the drying time of a liquid solvent layer moving on a conveyor and submitted to an air flow. The air can flow due to the conveyor motion and/or a jet from an air blade. The evaporation model takes into account mass transfers by convection and diffusion in air. The remaining mass of the liquid solvent along time and the drying time is then deduced.

The effect of convection on the drying time has been assessed numerically in three air flow configurations. It has been shown that increasing air velocity near the liquid layer leads to a decrease of the drying time. In an industrial production environment, the conveyor moves. In this context, it has been shown that in the presence of the jet, the drying time decreases dramatically by a factor 5, with demonstrates the interest of such device. This result allows considering using less volatile solvents using an air blade while reaching the same drying performances.

These results have been used as a proof of concept, and an experimental test bench is currently under building. Future works include a model-experiment vis-à-vis and optimizing the air blade.

Funding

This work has been founded by MARKEM-IMAJE and made in a fruitful collaboration between MARKEM-IMAJE and SIMTEC.

Acknowledgements

The authors thank gratefully Guillaume Paul for its experimental measurements and its expertise on the subject.

References

Castrejon-Pita, J. R., Baster, W. R., J., M., S., T., & M., M. G. (2013). Future, Opportunities and Challenges of Inket Technologies. *Atomization and Sprays*, *23*(6), 541-565.

COMSOL. (2020). COMSOL Multiphysics® v. 5.6. www.comsol.com. Stockholm, Sweden.

COMSOL. (2020). Numerical Stabilization. Dans COMSOL, *COMSOL Multiphysics, Reference Manual*,

COMSOL 5.6 (pp. 224-230).

Gaubert, Q. (2017). *Caractérisation et modélisation des phénomènes gouvernant le séchage par atomisation de suspensions colloïdales.* Phd thesis, Ecole doctorale 353.

Hughes, T. J., Franca, L. P., & Balestra, M. (1986, November). A new finite element formulation for computational fluid dynamics: V. Circumventing the babuška-brezzi condition: a stable Petrov-Galerkin formulation of the stokes problem accommodating equal-order interpolations. *Computer Methods in Applied Mechanics and Engineering, 59*(1), 85-99.

Le, H. P. (1999). Progress and Trends in Ink-jet Printing Technology. *Recent Progress in Ink Jet Technologies II*, 1-14.

Numata, M., Sakamoto, A., Ogasawara, Y., Hatanaka, M., Motosugi, Y., & Morita, N. (2013). Drying Technology Using Laser Exposure for High-speed Inkjet Printing. *NIP & Digital Fabrication Conference*.